



## Transport and relaxation of current-generated nonequilibrium phonons from nonlocal electronic measurements

Guanxiong Chen and Sergei Urazhdin 

*Department of Physics, Emory University, Atlanta, Georgia 30322, USA*

 (Received 9 July 2021; revised 17 December 2021; accepted 1 March 2022; published 15 March 2022)

We study phonons generated by current in a Pt nanowire by measuring the resistance of another nanowire separated from the first one by an insulating spacer. For thin spacers, the resistance varies almost linearly with current at cryogenic temperatures, while an additional quadratic contribution emerges for thicker spacers. These observations suggest a nonthermal distribution of current-generated phonons that relax via strongly nonlinear dynamical processes rather than few-phonon scattering. Our results provide insight into the nonequilibrium phonon dynamics at nanoscale, which may facilitate efficient heat management in electronic nanodevices.

DOI: [10.1103/PhysRevB.105.L100302](https://doi.org/10.1103/PhysRevB.105.L100302)

The rapidly increasing speed and functionalities of modern electronic devices are enabled by the increasing complexity and density of integrated circuits (ICs) facilitated by the continued downscaling of circuit elements [1]. The characteristic dimensions of transistors are reaching scales below 10 nm [2–4], approaching the fundamental limits of semiconductor technology [5]. Further density increases based, for example, on three-dimensional (3D) IC architectures [6–8] will require new approaches to efficient dissipation of Joule heat at nanoscale [9–11].

Current-generated phonons are commonly assumed to form a quasiequilibrium distribution characterized by a local effective temperature [12], as embodied by the interchangeable use of the terms “Joule dissipation” and “Joule heating” [13,14]. The former describes electric energy deposited in the material, while the latter implies that phonons form a thermal (Bose-Einstein) distribution and can be described as heat. However, the observation of linear dependence of resistance on current in metallic nanostructures indicated a nonequilibrium phonon distribution that cannot be characterized by an effective temperature [15]. Similar conclusions were reached in the studies of carbon nanotubes [16,17] and current-driven superconductivity suppression [18]. These findings suggest the possibility to optimize heat dissipation by utilizing a relatively small flux of nonthermalized (i.e., not described by the Bose-Einstein distribution) high-energy phonons.

Here, we present nonlocal electronic measurements utilizing a phonon-detecting nanowire separated from the phonon-generating wire by an electrically insulating spacer, Fig. 1(a). The separation between phonon generation and detection allows us to confirm nonthermal distribution of current-generated phonons, characterize inelastic phonon scattering, and elucidate its mechanisms. Our samples consisted of two 7-nm-thick, 1- $\mu\text{m}$ -wide, and 18- $\mu\text{m}$ -long Pt wires fabricated on top of one another on undoped Si substrates and contacted by Cu electrodes [20]. The large nanowire length ensured that phonon escape into the electrodes was negligible. The wires were separated by an insulating amorphous SiO<sub>2</sub> spacer

whose thickness  $d$  was varied between 5 and 100 nm. Similar behaviors were observed for crystalline MgO spacers [20] extensively utilized in magnetic tunnel junctions [21–24]. To generate phonons, dc current  $I_s$  was applied to the top wire. The resistance  $R_d$  of the bottom wire used as the phonon detector was measured using lock-in detection with a small ac current  $I_d = 10 \mu\text{A}$  applied to this wire. A small ac frequency  $f = 13 \text{ Hz}$  was used to minimize capacitive artifacts. Both wires were metallic with resistance of about 800  $\Omega$ , with negligible contribution from the contact resistance, as confirmed by separate four-probe measurements. The resistance between the Pt wires was at least 25 M $\Omega$  at cryogenic temperatures.

Figure 1(b) shows  $R_d(I_s)$  for two spacer thicknesses,  $d = 25 \text{ nm}$  and 100 nm, at temperature  $T = 300 \text{ K}$  [25]. To account for slight differences between samples, the data are offset and normalized by  $R_d(0)$ . The two data sets closely follow the same quadratic dependence. This result is consistent with Joule heating and Fourier’s law of heat diffusion. Indeed, the rate of electric energy dissipation per unit source wire area is  $w = d_{Pt} \rho j_s^2$ , where  $d_{Pt}$  is its thickness,  $j_s$  is the current density, and  $\rho$  is resistivity. For the studied thin-film wires, the latter is dominated by surface and impurity scattering, as evidenced by its weak dependence on  $T$  [Fig. 1(c)], so to the lowest order the variation of  $\rho$  with  $j_s$  can be neglected.

The dissipated energy produces a heat flux  $q = w$  flowing through the spacer and the sensing layer into the substrate, and spreading over the characteristic depth  $z_c$  defined by the wire width, as seen from the COMSOL simulation Fig. 1(d) [20]. In the 1D approximation, this can be modeled by a heat sink with the temperature  $T$  at the depth  $z_c$  below the sensing Pt wire. According to Fourier’s law,  $q = -\kappa \nabla T$ , where  $\kappa$  is the thermal conductivity of the substrate. We infer that the temperature of the detector wire  $T_d = T + z_0 d_{Pt} \rho j_s^2 / \kappa$  does not depend on the properties of the spacer and is quadratic in  $I_s$ . Above the Bloch-Grüneisen temperature  $\Theta_R \approx 50 \text{ K}$  [26], the resistance  $R_d$  of the detector wire is linear in  $T$  [Fig. 1(c)], so  $R_d$  is expected to be quadratic in  $I_s$ , in agreement with the

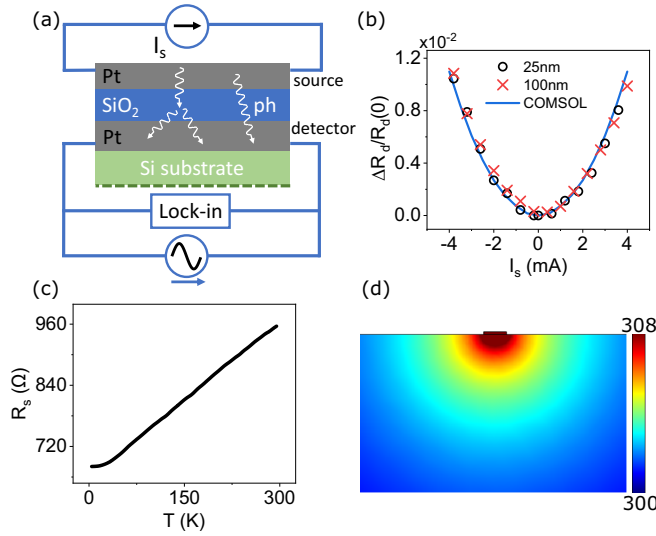


FIG. 1. (a) Schematic of the studied structures and measurement. (b)  $\Delta R_d/R_d(0)$  vs  $I_s$  for  $d = 25$  nm (circles) and  $100$  nm (crosses), at  $T = 300$  K. Here,  $\Delta R_d = R_d(I_s) - R_d(0)$ . Curve: COMSOL [19] simulation for  $d = 100$  nm. The result for  $d = 25$  nm (not shown) is nearly identical. (c)  $R_s$  vs  $T$  at  $I_s = 0$ . The dependence  $R_d(T)$  is similar. (d) Cross section of the temperature distribution calculated for  $d = 100$  nm, at  $I_s = 4$  mA and  $T = 300$  K.

data and the COMSOL [19] simulations based on Fourier's law [curve in Fig. 1(b)].

Similar analysis predicts a quadratic current dependence of the source resistance  $R_s$ , but with a coefficient that depends on the spacer. The resistivity of the Pt wires saturates below  $\Theta_R$ , Fig. 1(c). Therefore, for measurements performed at  $T \ll \Theta_R$ , Joule heating should result in almost constant  $R_s$  at small  $I_s$ , crossing over to a quadratic dependence at large  $I_s$ , as illustrated by the COMSOL [19] simulation [dashed curve in Fig. 2(a)] [20].

The dependence  $R_s(I_s)$  measured at  $T = 7$  K is qualitatively different from this prediction [symbols in Fig. 2(a)]. It can be precisely fitted by  $R_s(I) = R_s(0) + \gamma$ , where  $\gamma$  is a linear function of  $|I_s|$  convolved with a Gaussian of width  $\Delta I_s$ ,  $\gamma(\alpha, \Delta I_s, I_s) = \alpha \int dI |I| e^{-(I-I_s)^2/2\Delta I_s^2} / \sqrt{2\pi} \Delta I_s$  [solid curve in Fig. 2(a)] [27]. A similar result obtained in Ref. [15]

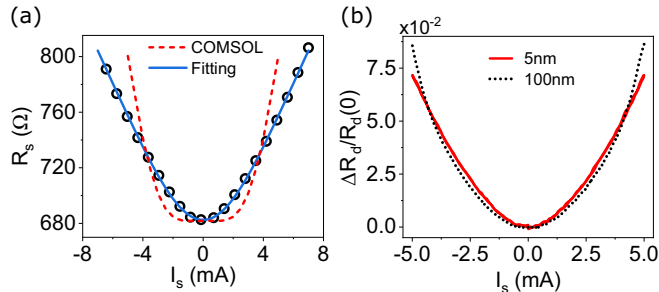


FIG. 2. (a)  $R_s$  vs  $I_s$  for  $d = 5$  nm, at  $T = 7$  K. Symbols: data; dashed curve: COMSOL simulation; solid curve: fitting with the function  $\gamma(\alpha, \Delta I_s, I_s)$  defined in the text. (b) Measured  $\Delta R_d/R_d(0)$  vs  $I_s$  for  $d = 5$  nm (solid curve) and  $100$  nm (dashed curve), at  $T = 7$  K. The measurement error is smaller than the linewidth.

was interpreted as evidence for the nonequilibrium distribution of current-generated phonons that cannot be described by an effective temperature. We now outline this interpretation. According to the Drude-Sommerfeld model, the rate of electron scattering in the source wire is proportional to  $I_s$ . Assuming that one phonon is generated in each electron scattering event, and neglecting the effects of inelastic scattering on the phonon population before they escape into the substrate, the kinetic balance relation gives a linear dependence of the current-generated phonon population on current [15]. Electron scattering on these phonons leads to a linear dependence  $R_s(|I_s|)$ .

In this picture, phonon distribution must be nonthermal by the energy conservation argument. The deposited electrical energy is quadratic in  $I_s$ , while the number of the generated phonons is proportional to  $|I_s|$  and thus the average energy per phonon is also proportional to  $|I_s|$ . The same conclusion is obtained by considering the energy imparted by electric bias to each electron between the scattering events, which must be transferred to the phonon generated upon scattering. The observed smoothing of the weak singularity at  $I_s = 0$  is then explained by the reduced cross section of electron scattering on the low-energy phonons generated at small  $I_s$ .

For the thermalized phonon distribution below the Debye temperature  $\Theta_D = 240$  K of Pt, the average phonon energy  $\langle \epsilon \rangle$  is linear in  $T$ , as follows from the Debye integral  $\langle \epsilon \rangle \propto \int_0^\infty (e^x - 1)^{-1} kT x^3 dx / \int_0^\infty (e^x - 1)^{-1} x^2 dx \propto T$ . Thus, for  $T_s \propto I_s^2$ ,  $\langle \epsilon \rangle \propto I_s^2$ . At  $T > \Theta_D$ , the average energy of thermalized phonons is independent of  $T$ , as follows from the Rayleigh-Jeans law for the thermal mode population,  $n(\epsilon) = kT/\epsilon$ . One concludes that the linear dependence of  $R_s$  on  $|I_s|$  is inconsistent with thermal distribution of current-generated phonons.

Nonlocal measurements provide a test for this interpretation. If the distribution of phonons injected into the spacer is nonthermal, their inelastic scattering is expected to result in gradual thermalization, i.e., redistribution of mode populations towards Bose-Einstein distribution. Thus the dependence  $R_d(I_s)$  should be close to linear for thin spacers and approach the form expected for Joule heating for thick spacers. Indeed, the measured  $R_d(I_s)$  for  $d = 5$  nm is close to the linear dependence  $R_s(I_s)$ , while for  $d = 100$  nm it is close to parabolic [Fig. 2(b)]. As a consequence, at small  $I_s$  the normalized  $R_d$  is larger for  $d = 5$  nm than for  $d = 100$  nm, and smaller at large  $I_s$ , with a crossover at  $|I_s| = 4$  mA.

All the  $R_d$  vs  $I_s$  curves obtained at  $T = 7$  K are well approximated by the sum of the function  $\gamma(\alpha, \Delta I_s, I_s)$  used for fitting the local measurements, with the same value of  $\Delta I_s$ , and the quadratic function  $\beta I_s^2$  [inset in Fig. 3(a)]. The former describes the “primary” phonons generated in the source wire that diffuse to the detector without experiencing thermalizing inelastic scattering. The quadratic contribution reflects the presence of a “secondary” group of phonons generated in the spacer due to inelastic scattering of the “primary” phonons [28].

The linear contribution exponentially decreases with increasing  $d$ , with the decay length  $d_0 = 44 \pm 2$  nm, Fig. 3(a). The quadratic contribution increases with increasing  $d$ , which can be also described by the same exponential form, Fig. 3(b). These results are consistent with the effects of inelastic

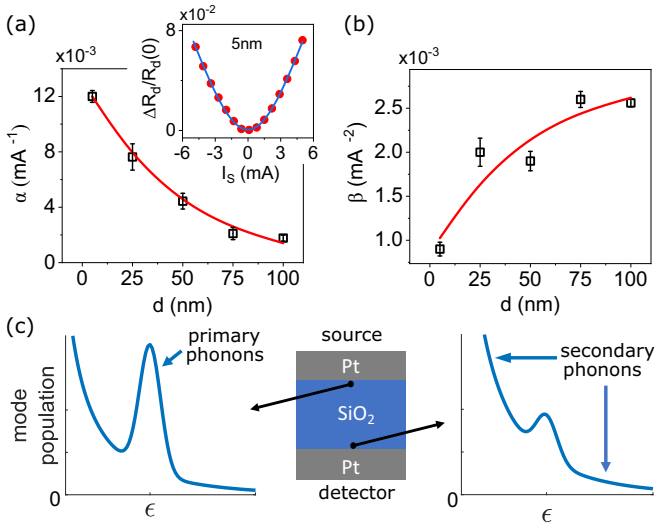


FIG. 3. (a),(b) Amplitudes  $\alpha$  (a) and  $\beta$  (b) of the linear and the quadratic contributions to  $R_d(I_s)$  vs  $d$ , determined from fittings such as those shown in the inset for  $d = 5$  nm and  $T = 7$  K. Curves are fittings with the exponential dependences  $\alpha_0 e^{-d/d_0}$  in (a) and  $\beta_0 - \beta_1 e^{-d/d_0}$  in (b), with the same  $d_0 = 44$  nm. (c) Schematic of the phonon mode population vs mode energy close the source (left) and the detector (right).

scattering in the spacer that decreases the primary phonon population and increases the secondary phonon population, as schematically shown in Fig. 3(c) for two local phonon distributions in the spacer—one close to the source wire and another to the detector.

We note that the quadratic contribution extrapolates to a finite  $\beta(0) = 8 \times 10^{-4} \text{ mA}^{-2}$ , indicating that the secondary phonons are also generated at the Pt/SiO<sub>2</sub> interfaces. We can estimate the probability  $P_{el}$  that the primary phonon is transmitted elastically across the Pt/SiO<sub>2</sub> interface by using the extrapolated value  $\beta(\infty) = 2.8 \times 10^{-3} \text{ mA}^{-2}$ . Accounting for the two Pt/SiO<sub>2</sub> interfaces separating the source from the detector, we obtain  $P_{el}^2 = 1 - 8/28$ , i.e.,  $P_{el} = 0.85$ .

Based on the energy conservation arguments discussed above, the density  $n_1$  of the primary phonons and their average quasiparticle energy  $\epsilon_1$  are proportional to  $|I_s|$ . The distribution of the primary phonons is schematically shown in Fig. 3(c) as a peak, while the secondary phonon distribution is approximated as Bose-Einstein distribution. The quadratic dependence  $R_d(I_s)$  for the secondary phonons means that their density  $n_2$  is quadratic in  $I_s$ , so their average energy  $\epsilon_2$  is independent of  $I_s$ . At  $T > \Theta_D$ , this would be indeed consistent with the degenerate Bose-Einstein distribution. However, for thermalized phonons at  $T = 7 \text{ K} \ll \Theta_D$ ,  $\epsilon \propto I_s^2$  (see above), i.e., the secondary phonons are not thermalized. This is not surprising since, at least for thin spacers, phonons are expected to experience only a few scattering events before escaping into the substrate. Meanwhile, thermalization requires many scattering events that change the phonon population and redistribute their momentum and energy.

To analyze inelastic scattering that results in the generation of secondary phonons, we consider the continuity equations in the relaxation time approximation,  $\partial n_1/\partial t =$

$-\nabla \cdot \mathbf{f}_1 - n_1/\tau_{in}$  for the primary phonons and  $\partial n_2/\partial t = -\nabla \cdot \mathbf{f}_2 + n_1 \epsilon_1/\tau_{in} \epsilon_2$  for the secondary phonons. Here,  $\mathbf{f}_{1,2}$  are the quasiparticle fluxes, and we used energy conservation to relate the secondary phonon generation to the annihilation rate  $1/\tau_{in}$  of the primary phonons. In the diffusive phonon transport approximation justified by the small phonon MFP  $l_{el} \approx 5$  nm in amorphous SiO<sub>2</sub> at cryogenic  $T$  [29,30],  $\mathbf{f}_{1,2} = -D\nabla n_{1,2}$ , where  $D = v_{ph} l_{el}/3$  is the diffusion coefficient and  $v_{ph}$  is the phonon group velocity, which can be approximated by the sound velocity  $\approx 4.5$  km/s in amorphous SiO<sub>2</sub>. Thus we estimate  $D \approx 7.5 \times 10^{-6} \text{ m}^2/\text{s}$ .

The phonon distribution in the spacer depends only on the coordinate  $z$  directed into the substrate, whose origin is set in the SiO<sub>2</sub> spacer at the boundary with the source. For the stationary state, we obtain

$$\begin{aligned} n_1(z) &= n_1^{(0)} e^{-z/\sqrt{D\tau_{in}}}, \\ n_2(z) &= n_1^{(0)} \frac{\epsilon_1}{\epsilon_2} + \left( n_2^{(0)} - n_1^{(0)} \frac{\epsilon_1}{\epsilon_2} \right) e^{-z/\sqrt{D\tau_{in}}}, \end{aligned} \quad (1)$$

where  $n_1^{(0)}$  ( $n_2^{(0)}$ ) is the primary (secondary) phonon density at  $z = 0$ . These dependences are consistent with the observed variations of  $\alpha$  and  $\beta$  [Fig. 3(b)], allowing us to estimate the inelastic scattering time  $\tau_{in} = d_0^2/D = 270$  ps. The inelastic scattering length, defined as the total phonon path between inelastic scattering events, is  $l_{in} = \tau_{in} v_{ph} = 1.2 \mu\text{m}$ . This value is much smaller than the sound attenuation length characterizing low-frequency acoustic waves, but is still promising for optimizing thermal management in nanodevices by using transport of nonthermalized phonons.

We now analyze the mechanisms of secondary phonon generation. Inelastic scattering is usually described in terms of few-phonon processes governed by the quasiparticle energy and momentum conservation [31–33]. In these processes, the average energies of the generated phonons linearly scale with those of the annihilated phonons, which is inconsistent with our results. A cascade of few-phonon scattering could result in thermalization. However, this cannot explain similar behaviors observed over a wide range of spacer thicknesses. Damping of long-wavelength acoustic wave can be described by the diffusive Akhiezer mechanism associated with the strain-induced modulation of phonon spectrum [34]. This quasiadiabatic mechanism is relevant to long-wavelength phonons propagating over macroscopic distances, but not to the high-energy phonons studied in this work [20].

Since inelastic scattering requires anharmonicity, but weak anharmonicity underlying the few-phonon processes cannot account for our observations, we conclude that secondary phonons are likely generated due to strongly anharmonic dynamics. In crystalline materials, such dynamics may be associated with dislocations and local impurities, as well as incoherent interfaces [35,36]. Anharmonic dynamics in amorphous materials is generally expected due to the metastable structure and may be related to the bosonic spectral peak [37–39] and to the problem of phonon glass [40,41].

Here, we consider for concreteness a bistable atomic configuration, Fig. 4(a). Such bistable states result in the ubiquitous  $1/f$  noise present even in crystalline materials [42] and are likely abundant in amorphous SiO<sub>2</sub>. To model phonon scattering by a bistable defect, we consider a wave packet

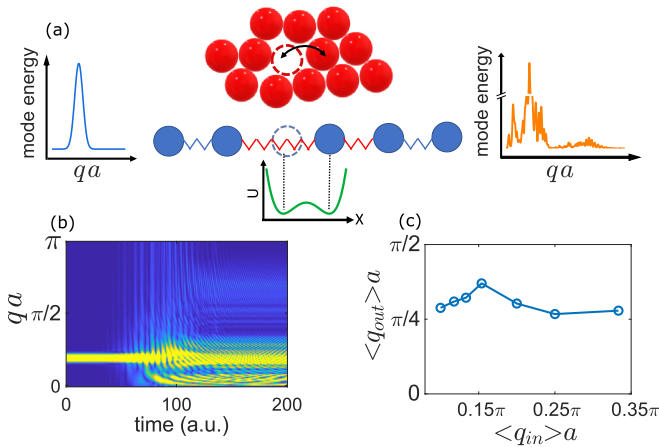


FIG. 4. (a) Schematic of the 1D simulation of inelastic phonon scattering by a strongly anharmonic defect as a chain of masses connected by springs. Top inset: example of a strongly anharmonic defect associated with a bistable atomic position in amorphous solid. Bottom inset: potential vs displacement for the mass  $n_0$  attached to the anharmonic springs. Left (right) inset: mode energy vs wave vector times the lattice constant for the phonon wave packet before (after) scattering. (b) Wave vector distribution vs time during phonon scattering on the defect. (c) Average wave vector of the generated phonon modes vs incident phonon wave vector, obtained by cutting out twice the Gaussian width around the wave packet center after scattering.

propagating along a 1D ring of masses  $n = 1-300$  connected to their neighbors by springs [Fig. 4(a)]. All the springs are linear with the same spring constant, except the two springs connected to the mass  $n_0 = 150$  are described by the double-

well potential energy  $U(x) = -k_1x^2/2 + k_3x^4/4$ , resulting in bistable equilibrium of mass  $n_0$  [bottom inset in Fig. 4(a)].

Dynamics spanning both potential wells cannot be described by the perturbative anharmonic expansion, because of the saddle point of the potential at  $x = 0$ . Wave packet scattering on the defect results in the generation of a broad range of modes throughout the entire Brillouin zone, Fig. 4(b), instead of the harmonics expected for weak anharmonicity [43]. The average wave vector of the generated modes remains almost constant when the center wave vector of the incident wave packet is varied by more than a factor of 5 [Fig. 4(c)], consistent with our experimental observations. This result indicates a breakdown of the perturbative picture [44], enabling nonresonant scattering not constrained by the usual quasiparticle momentum and energy conservation laws.

Our model serves as a simple illustration of the proposed phonon relaxation by strongly anharmonic scattering. We expect that future more rigorous analysis will shed light on the microscopic mechanisms relevant to specific materials. For amorphous materials, it must include diffusons, locons, and propagons [41,45], beyond the scope of this work.

In summary, we utilized nonlocal electronic measurements to show that a highly nonthermal distribution of phonons is generated by electric current in nanostructures at cryogenic temperatures. We demonstrated an approach for the characterization of their inelastic scattering and used it to demonstrate that the latter is dominated by strongly anharmonic, nonperturbative processes. Our results suggest heretofore unexplored routes for optimizing heat management in electronic nanodevices.

We thank V. Perebeinos for a helpful discussion. Measurements performed by G.C. were supported by the U.S. DOE BES Award No. DE-SC0018976. Analysis was supported by the NSF Grant No. ECCS-1804198.

- [1] Y.-Y. Noh, N. Zhao, M. Caironi, and H. Siringhaus, *Nat. Nanotechnol.* **2**, 784 (2007).
- [2] J. Martinez, R. V. Martinez, and R. Garcia, *Nano Lett.* **8**, 3636 (2008).
- [3] S. B. Desai, S. R. Madhupathy, A. B. Sachid, J. P. Llinas, Q. Wang, G. H. Ahn, G. Pitner, M. J. Kim, J. Bokor, C. Hu *et al.*, *Science* **354**, 99 (2016).
- [4] H. Ilatikhameneh, T. Ameen, B. Novakovic, Y. Tan, G. Klimeck, and R. Rahman, *Sci. Rep.* **6**, 31501 (2016).
- [5] D. Mamaluy and X. Gao, *Appl. Phys. Lett.* **106**, 193503 (2015).
- [6] S. Wong, A. El-Gamal, P. Griffin, Y. Nishi, F. Pease, and J. Plummer, in *2007 International Symposium on VLSI Technology, Systems and Applications (VLSI-TSA)* (IEEE, New York, 2007), pp. 1–4.
- [7] P. D. Franzon, W. R. Davis, M. B. Steer, S. Lipa, E. C. Oh, T. Thorolfsson, S. Melamed, S. Luniya, T. Doxsee, S. Berkeley *et al.*, in *2008 45th ACM/IEEE Design Automation Conference* (IEEE, New York, 2008), pp. 668–673.
- [8] J. Knechtel, O. Sinanoglu, I. A. M. Elfadel, J. Lienig, and C. C. Sze, *IPSI Trans. Syst. LSI Design Methodol.* **10**, 45 (2017).
- [9] D. Sekar, C. King, B. Dang, T. Spencer, H. Thacker, P. Joseph, M. Bakir, and J. Meindl, in *2008 International Interconnect Technology Conference* (IEEE, New York, 2008), pp. 13–15.
- [10] S. Wang, Y. Yin, C. Hu, and P. Rezai, *Micromachines* **9**, 287 (2018).
- [11] J. Xie and M. Swaminathan, *IEEE Trans. Components Packag. Manufact. Technol.* **1**, 234 (2011).
- [12] The adjective “effective” reflects the fact that temperature is a rigorous characteristic only in true equilibrium.
- [13] S. S. Ghai, W. T. Kim, R. A. Escobar, C. H. Amon, and M. S. Jhon, *J. Appl. Phys.* **97**, 10P703 (2005).
- [14] A. Nabovati, D. P. Sellan, and C. H. Amon, *J. Comput. Phys.* **230**, 5864 (2011).
- [15] G. Chen, R. Freeman, A. Zholud, and S. Urazhdin, *Phys. Rev. X* **10**, 011064 (2020).
- [16] Z. Yao, C. L. Kane, and C. Dekker, *Phys. Rev. Lett.* **84**, 2941 (2000).



- [17] L. Siddiqui, A. W. Ghosh, and S. Datta, *Phys. Rev. B* **76**, 085433 (2007).
- [18] M. F. Ritter, N. Crescini, D. Z. Haxell, M. Hinderling, H. Riel, C. Bruder, A. Fuhrer, and F. Nichele, *Nature Electron.* **5**, 71 (2022).
- [19] COMSOL Multiphysics® v. 5.6, [www.comsol.com](http://www.comsol.com), COMSOL AB, Stockholm, Sweden.
- [20] See Supplemental Material at <http://link.aps.org/supplemental/10.1103/PhysRevB.105.L100302> for MgO spacer, dependence on temperature, analysis of phonon energies, and simulation details.
- [21] S. Yuasa, T. Nagahama, A. Fukushima, Y. Suzuki, and K. Ando, *Nat. Mater.* **3**, 868 (2004).
- [22] S. S. P. Parkin, C. Kaiser, A. Panchula, P. M. Rice, B. Hughes, M. Samant, and S.-H. Yang, *Nat. Mater.* **3**, 862 (2004).
- [23] J. Hayakawa, S. Ikeda, F. Matsukura, H. Takahashi, and H. Ohno, *Jpn. J. Appl. Phys.* **44**, L587 (2005).
- [24] S. S. Mukherjee, F. Bai, D. MacMahon, C.-L. Lee, S. K. Gupta, and S. K. Kurinec, *J. Appl. Phys.* **106**, 033906 (2009).
- [25] Room-temperature measurements for  $d < 25$  nm were unreliable because of electron activation across spacer.
- [26] C. Kittel, P. McEuen, and P. McEuen, *Introduction to Solid State Physics* Vol. 8 (Wiley, New York, 1996).
- [27] Phonon generation due to electron-phonon scattering can be neglected, since resistance is dominated by scattering at the boundaries and defects even at large bias.
- [28] Estimates discussed in the Supplemental Material suggest that both the primary and the secondary phonons are acoustic.
- [29] L. Yang, Q. Zhang, Z. Cui, M. Gerboth, Y. Zhao, T. T. Xu, D. G. Walker, and D. Li, *Nano Lett.* **17**, 7218 (2017).
- [30] C. Kittel, *Phys. Rev.* **75**, 972 (1949).
- [31] J. M. Ziman, *Electrons and Phonons: The Theory of Transport Phenomena in Solids* (Oxford University Press, Oxford, 2001).
- [32] Y. Guo, M. Bescond, Z. Zhang, M. Luisier, M. Nomura, and S. Volz, *Phys. Rev. B* **102**, 195412 (2020).
- [33] R. Yang, S. Yue, Y. Quan, and B. Liao, *Phys. Rev. B* **103**, 184302 (2021).
- [34] A. Akhiezer, *J. Phys. (Moscow)* **1**, 277 (1939).
- [35] R. O. Pohl, X. Liu, and E. Thompson, *Rev. Mod. Phys.* **74**, 991 (2002).
- [36] M. Molina-Ruiz, H. Jacks, D. Queen, T. Metcalf, X. Liu, and F. Hellman, *Phys. Rev. B* **104**, 024204 (2021).
- [37] L. Zhang, Y. Wang, Y. Chen, J. Shang, A. Sun, X. Sun, S. Yu, J. Zheng, Y. Wang, W. Schirmacher, and J. Zhang, *Phys. Rev. Res.* **3**, L032067 (2021).
- [38] S. Mahajan and M. P. Ciamarra, *Phys. Rev. Lett.* **127**, 215504 (2022).
- [39] Z.-Y. Yang, Y.-J. Wang, and A. Zacccone, *Phys. Rev. B* **105**, 014204 (2022).
- [40] J. L. Feldman, M. D. Kluge, P. B. Allen, and F. Wooten, *Phys. Rev. B* **48**, 12589 (1993).
- [41] P. B. Allen, J. L. Feldman, J. Fabian, and F. Wooten, *Philos. Mag. B* **79**, 1715 (1999).
- [42] P. Dutta and P. M. Horn, *Rev. Mod. Phys.* **53**, 497 (1981).
- [43] L. D. Landau and E. M. Lifshitz, *Mechanics, Third Edition: Volume 1 (Course of Theoretical Physics)* (Butterworth-Heinemann, London, 1976).
- [44] J. Moon, *J. Appl. Phys.* **130**, 055101 (2021).
- [45] A. Cepellotti and N. Marzari, *Phys. Rev. X* **6**, 041013 (2016).